

2MASS J04435686+3723033 B: A Young Companion at the Substellar Boundary with Potential Membership in the β Pictoris Moving Group

Caprice L. Phillips ^{1,5} , Brendan P. Bowler ² , Gregory Mace ³ , Michael C. Liu ⁴ , and Kimberly Sokal ³ Department of Astronomy, The Ohio State University, Columbus, OH 43210, USA ² Department of Astronomy, The University of Texas at Austin, Austin, TX 78712, USA ³ McDonald Observatory & Department of Astronomy, University of Texas at Austin, 2515 Speedway, Stop C1400, Austin, TX 78712-1205, USA ⁴ Institute for Astronomy, University of Hawai'i at Mānoa, 2680 Woodlawn Drive, Honolulu, HI 96822, USA **Received 2019 July 23; revised 2020 April 6; accepted 2020 April 7; published 2020 June 25

Abstract

We present a detailed characterization of 2MASS J04435750+3723031, a low-mass companion orbiting the young M2 star 2MASS J04435686+3723033 at 7."6 (550 au) with potential membership in the 23 Myr β Pictoris moving group (β PMG). Using near-infrared (NIR) spectroscopy of the companion from IRTF/SpeX, we have found a spectral type of M6 \pm 1 and indications of youth through age-sensitive absorption lines and a low surface gravity index (VL-G). A young age is supported by H α emission and lithium absorption in the host. We reevaluate the membership of this system and find that it is a marginally consistent kinematic match to the β PMG using Gaia parallaxes and new radial velocities for the host and companion. If this system does belong to the β PMG, it would be a kinematic outlier and the companion would be overluminous compared to other similar ultracool objects like PZ Tel B; this would suggest that 2M0443+3723 B could be a close binary (\approx 52+52 $M_{\rm Jup}$ if equal-flux, compared with 99 \pm 5 $M_{\rm Jup}$ if single), and would make it the sixth substellar companion in this group. To test this hypothesis, we acquired NIR adaptive optics images with Keck II/NIRC2, but they do not resolve the companion to be a binary down to the diffraction limit of \sim 3 au. If 2M0443+3723 AB does not belong to any moving group, then its age is more uncertain. In this case it is still young (\lesssim 30 Myr), and the implied mass of the companion would be between \sim 30 and 110 $M_{\rm Jup}$.

Unified Astronomy Thesaurus concepts: Low mass stars (2050); Brown dwarfs (185); Direct imaging (387); Close binary stars (254)

Supporting material: data behind figures

1. Introduction

The study and characterization of the lowest-mass stars and brown dwarfs (BDs) is a relatively new field, with the first BDs, Gliese 229 B (Nakajima et al. 1995; Oppenheimer et al. 1995), Teide 1 (Rebolo et al. 1995), and PPL 15 (Basri et al. 1996), having been discovered less than a quarter century ago. BDs $(\lesssim 75 M_{\text{Jup}})$ are not massive enough to stably burn hydrogen in their cores and thus represent the transition region between gas giant planets and low-mass stars. Substellar objects that fall below the hydrogen-burning limit gradually cool and grow dimmer as they age and thus follow a degenerate mass-ageluminosity relationship (Burrows et al. 2001; Saumon & Marley 2008). This is contrary to low-mass stars, which have stable luminosities over the main course of their lifetime. These objects are generally defined based on the limit for the onset of hydrogen and deuterium burning, not necessarily their formation: stars have masses greater than 75 M_{Jup} , BDs span 13-75 M_{Jup} , and objects between 0.2 and 13 M_{Jup} are considered gas giant planets if they are companions to stars (Burrows et al. 2001).

Benchmark systems are objects that have two or more measured fundamental quantities such as luminosity and age; for BDs these parameters can be used to infer other properties like mass, temperature, and radius using substellar evolutionary models (Burrows et al. 2001). For example, BDs that are companions to stars and members of young moving groups (YMGs) have ages that can be determined from the age of the host star or from age-dating the moving group. Benchmark BDs

provide valuable tests for substellar atmospheric and evolutionary models by anchoring parameters to provide assessments for mutual consistency or to serve as direct comparisons with predictions from ultracool atmospheric and evolutionary models (e.g., Bowler et al. 2009; Dupuy et al. 2009; Crepp et al. 2012; Brandt et al. 2019).

Similarly, young low-mass stars with well-constrained ages and metallicities offer important tests of pre-main-sequence evolutionary models (e.g., Montet et al. 2015; Nielsen et al. 2016). There is growing evidence for discrepancies between the measured properties of young low-mass stars and predictions from evolutionary tracks (e.g., Kraus et al. 2015; David et al. 2015; Rizzuto et al. 2017), which may point to a systematic error in the modeling of convective stars. For example, Feiden (2016) found that including magnetic fields in the evolution of lowmass stars inhibits their convection and slows their contraction along the Hayashi track. This puts the inferred isochronal ages for K and M dwarfs more in line with those for earlier-type stars of the same cluster and appears to largely reconcile the inferred masses determined from H-R diagrams with dynamical masses (Simon et al. 2019). Identifying the lowest-mass stellar and substellar members of young clusters is therefore important to continue these tests over a variety of cluster ages, sizes, and environments.

Over the past few years, new high-contrast adaptive optics (AO) imaging instruments have paved the way for direct imaging studies of exoplanets and BD companions (Bowler 2016). The Spectro-Polarimetric High-contrast Exoplanet REsearch (SPHERE; Beuzit et al. 2008) instrument at the Very Large Telescope (VLT), Subaru Coronographic Extreme

⁵ LSSTC DSFP Fellow.

Adaptive Optics (SCExAO; Martinache et al. 2014), MagAO-X (Males et al. 2018), Gemini Planet Imager (GPI; Macintosh et al. 2014), and the Near-infrared Coronagraphic Imager (NICI; Chun et al. 2008) at Gemini-South have made imaging BDs and exoplanet companions more accessible. With the development of these specialized instruments, several BDs and planets have been discovered with direct imaging (e.g., Marois et al. 2008; Biller et al. 2010; Macintosh et al. 2015), but a detailed study of their atmospheres is difficult because they reside so close to their host stars. The upcoming development of larger telescopes such as the James Webb Space Telescope, the European Extremely Large Telescope, and the Giant Magellan Telescope will be able to probe even closer separations and discover lower-mass planets to characterize their fundamental properties. However, detailed, high signal-tonoise ratio (S/N) spectroscopy of these objects will be difficult, underscoring the value of wide substellar companions that are free of contamination from their host stars.

Nearby YMGs represent some of the best regions to identify intermediate-age benchmark BDs and low-mass stars. In these associations, the metallicities and ages of substellar companions are known because their members can generally be studied in detail (e.g., Biller et al. 2013; Naud et al. 2013). Members of these young, loose associations are ideal targets for directly imaging exoplanets in contrast to young star-forming clusters and unassociated nearby young stars, as the distances of YMGs are closer (≤100 pc) and the ages are well established (e.g., Zuckerman & Song 2004: Torres et al. 2006, 2008; Kraus et al. 2014).

The β Pictoris Moving Group (β PMG) is an intermediate-age (23 ± 3 Myr) cluster of stars that lies in the solar neighborhood (Zuckerman et al. 2001; Torres et al. 2008; Mamajek & Bell 2014). This association has a large spatial distribution in the sky, but its members share similar kinematics, which allows for stars to be identified as a common cluster in velocity space. Schlieder et al. (2010) proposed several new members of the β PMG based on proper motions, signatures of youth (e.g., H α and X-ray emission), and radial velocity (RV) measurements. In this study we examine one system in detail, 2M0443+3723 AB, which comprises an early M-type primary (2MASS J04435686+3723033, hereafter 2M0443+3723 A) and a mid- to late M secondary (2MASS J04435750+3723031, hereafter 2M0443+3723 B).

The companion, 2M0443+3723 B, is separated by 7.''6 (550 au) from the M2 host, and a spectral type of M5 is estimated by Schlieder et al. (2010) based on the inferred absolute magnitudes. In a study of low-mass objects in the β PMG, Messina et al. (2017) find that the 2M0443+3723 AB system deviated ($>3\sigma$) from other confirmed β PMG members in two components of the space velocity. However, Shkolnik et al. (2017) include the system as members of the β PMG in their ACRONYM survey. Because it is a potential new benchmark BD companion, our goal is to understand its properties and reassess its membership in the β PMG and other moving groups.

In Section 2 we describe the observations and data reduction. We summarize our results in Section 3, assess the membership in Section 4, and conclude in Section 5.

2. Observations

2.1. IRTF/SpeX

We obtained a near-infrared (NIR) spectrum of 2M0443 +3723 B using the short-wavelength cross-dispersed (SXD) mode on the SpeX spectrograph (Rayner et al. 2003), which is

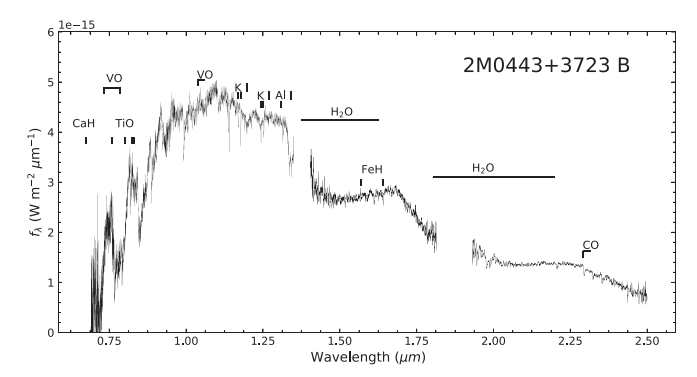


Figure 1. Our medium-resolution ($R \sim 750$) flux-calibrated 0.7–2.4 μ m spectrum of 2M0443+3723 B from IRTF/SpeX. We derive a M6 \pm 1 spectral type following Allers & Liu (2013). The low-S/N regions have been removed. (The data used to create this figure are available.)

located on the NASA Infrared Telescope Facility (IRTF) on Maunakea, Hawai'i. The SXD mode covers the $0.7-2.4\,\mu\mathrm{m}$ wavelength range and has a resolving power of $R\sim2000$ for a 0."3 slit width (or $R\sim750$ for a 0."8 slit). The data were obtained on 2015 November 28 UT using the 0."8 \times 15" slit with a total exposure time of 717 s. The observations were taken using consecutive ABBA nods and reduced using the SpeXTool package with the A0V standard HD 22859 (Vacca et al. 2003; Cushing et al. 2004). This reduction package extracts the spectra, performs wavelength calibration, corrects for telluric features using an A0V star, and merges the SXD orders. Our final medium-resolution ($R\sim750$) merged spectrum of 2M0443+3723 B is shown in Figure 1.

2.2. Discovery Channel Telescope/IGRINS

High-resolution NIR spectra of 2M0443+3723 A and 2M0443+3723 B were obtained with IGRINS (Immersion Grating Infrared Spectrometer; Park et al. 2014) at the 4.3 m Discovery Channel Telescope on 2017 September 02 UT. Observing conditions were partly cloudy. IGRINS simultaneously covers H and K bands with $R \sim 45,000$. 2M0443 +3723 A was observed in an ABBA quad sequence with individual exposure times of 300 s and a total integration time of 1200 s. 2M0443+3723 B was observed in an ABBAAB pattern with each exposure lasting 900 s for a total integration time of 5400 s. The data were reduced using the IGRINS pipeline package (Lee et al. 2017), which rectifies the 2D image and optimally extracts the spectra, performs wavelength calibration with OH lines, and corrects for telluric features with standard A0V stars (in this case HR 1692 and HR 1237).

2.3. Keck II/NIRC2 Adaptive Optics Imaging

Natural guide star (NGS) AO images of the 2M0443+3723 AB system were obtained on 2017 October 10 UT with the NIRC2 NIR imaging camera mounted on the Keck II $10 \,\mathrm{m}$ telescope. The companion was positioned in the top left quadrant of the detector, as the bottom left quadrant has increased noise levels. The host star was positioned in the bottom right quadrant of the detector. We obtained a total of six images of the system in the Maunakea Observatories (MKO) *H*-band filter (Simons & Tokunaga 2002; Tokunaga et al. 2002; Tokunaga & Vacca 2007) in narrow camera mode, which produces a plate scale of $9.971 \pm 0.004 \,\mathrm{mas}$ pixel $^{-1}$ (Service et al. 2016) and a field of

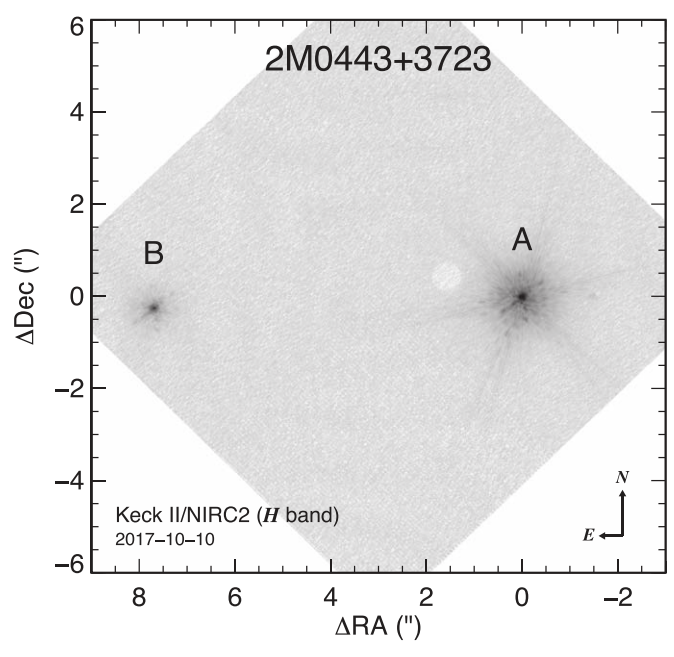


Figure 2. Keck II/NIRC2 AO image of 2M0443+3723 AB in H band.

view of $10.^{\prime\prime}2 \times 10.^{\prime\prime}2$. Each image is composed of 10 unsaturated co-adds with 2 s per co-add, resulting in a total on-source integration time of 20 s.

We perform basic image reduction including bias subtraction, flat-field division, bad pixel correction, and removal of cosmic rays using the <code>cosmics.py</code> package (van Dokkum 2001) in PYTHON, which utilizes Laplacian edge detection to identify and remove cosmic rays in the raw science frames. An example of a reduced image of the pair is shown in Figure 2.

3. Properties of the 2M0443+3723 AB System

3.1. Overview of 2M0443+3723 A

The host star, 2M0443+3723 A, has a spectral type of M2 \pm 1 as measured by Schlieder et al. (2010) and a distance of 71.6 \pm 0.3 pc (Gaia Collaboration et al. 2018). A similar photometric spectral type of M3 was determined by Shkolnik et al. (2017) in their ACRONYM survey. Messina et al. (2017) measured an H α emission equivalent width (EW) of -4.60 ± 0.21 Å. Malo et al. (2014) report a 194 \pm 4 mÅ EW of the Li I λ 6708 absorption feature. Bowler et al. (2019) find similar values of EW(H α) = -4.3 ± 0.9 Å and EW(Li I) = 0.12 ± 0.02 Å (Figure 3).

3.2. Empirical Comparison to Cool and Ultracool Dwarfs

To determine the spectral type of 2M0443+3723 B, we compare our SXD spectrum to the SpeX prism library of M, L, and T dwarfs (Burgasser 2014). We convolve our medium-resolution spectrum ($R \sim 750$) with a 1D Gaussian kernel to match the resolving power of the SpeX prism library ($R \sim 250$) and resample them to a common wavelength grid. Each prism spectrum was optimally scaled to our SXD spectrum via reduced χ^2 minimization,

$$\chi^2 = \sum_{i=0}^{n-1} \frac{(O_i - cE_i)^2}{\sigma_i^2},\tag{1}$$

where O_i is the flux density of the 2M0443+3723 B spectrum at pixel i, E_i is the flux density from the SpeX prism templates,

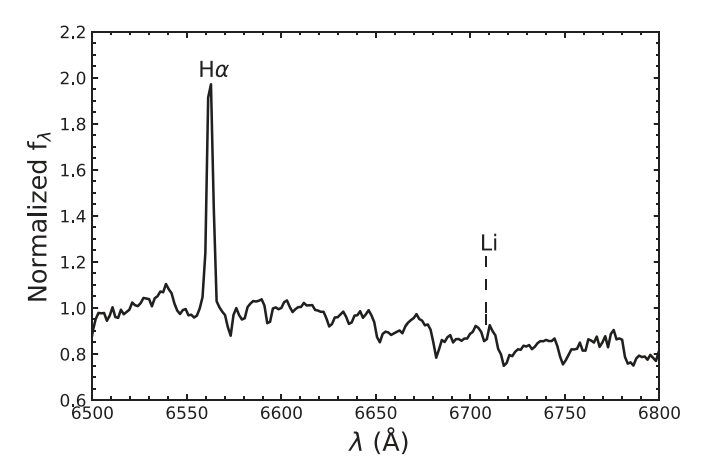


Figure 3. Optical spectrum of 2M0443+3723 A obtained from the RC-Spec instrument at the Mayall telescope, from Bowler et al. (2019). The spectrum has been normalized around 6600 Å. The H α emission indicates signs of chromospheric activity and serves as a necessary but not sufficient condition for youth. The lithium absorption feature at 6708 Å is also present, which unambiguously confirms the young age of the system.

(The data used to create this figure are available.)

and σ_i is the uncertainty associated with our 2M0443+3723 B spectrum. For each spectrum the optimal scale factor, c, is found following Cushing et al. (2008) to scale the prism templates to our SXD spectrum:

$$c = \frac{\sum O_i E_i / \sigma_i^2}{\sum E_i^2 / \sigma_i^2}.$$

In order to determine the goodness of fit between the prism library and our SXD spectrum, we utilize the reduced χ^2 statistic, $\chi^2_{\nu} \equiv \chi^2/\nu$, where ν represents the number of degrees of freedom (Figure 4). The best-fitting spectral type found from this analysis is M7 \pm 1. The best-fitting object from this method is 2MASS J00013044+1010146 (Figure 5; $\chi^2_{\nu} = 27.67$) (Burgasser et al. 2004). Witte et al. (2011) used the DRIFT-PHOENIX atmospheric models to find the best-fitting parameters for 2MASS J00013044+1010146, which suggested that it has a low surface gravity of log g=4.5 dex, $T_{\rm eff}=2900$ K, and M/H = +0.3 dex. Gagné et al. (2014) found an NIR spectral type of M6 and noted this object as being potentially young owing to low-gravity spectroscopic signs.

3.2.1. Index-based Spectral Type and Surface Gravity

Many features in the NIR spectra of BDs are influenced by gravity and age, for example, FeH (0.99, 1.20, 1.55 μ m), VO (1.06 μ m), K I (1.17 μ m), Na I (1.14, 2.21 μ m), and the *H*-band continuum shape (Allers & Liu 2013, hereafter AL13). AL13 developed an index-based spectral classification method based on visual classification, as well as flux ratios of NIR indices centered on spectroscopic features influenced by gravity and age. The visual classification method yields a spectral type of M6 \pm 1 from both the *J*-band and *H*-band regions. The overall spectral type is M6 \pm 1, with a gravity class of "VL-G" (very low gravity), which supports a young age for 2M0443+3723 B. We adopt the index-based spectral type from AL13 because the results are anchored to quantitative definitions, whereas the χ^2 spectral type depends on the author's spectral classification. Following the AL13 method, a score of 0–2 is assigned for

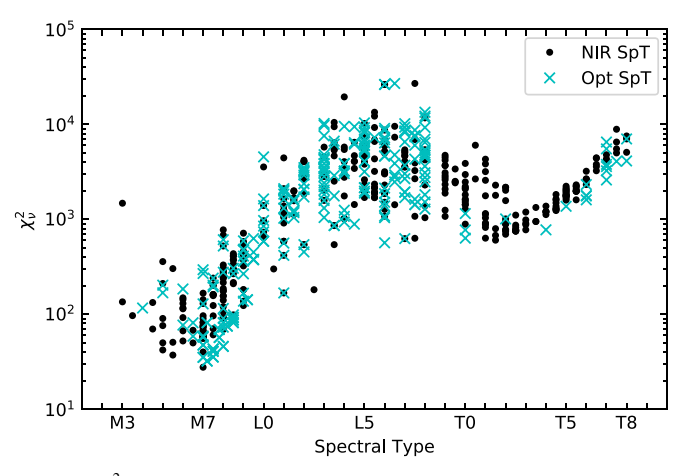


Figure 4. χ^2_{ν} comparison between cool and ultracool (\geqslant M6) dwarfs from the SpeX prism library and our spectrum of 2M0443+3723 B. Optical spectral types are shown with cyan symbols, and the NIR spectral types are shown with black circles. The closest match is that of 2MASS J00013044+1010146, which has an M7 NIR spectral type (Burgasser et al. 2004).

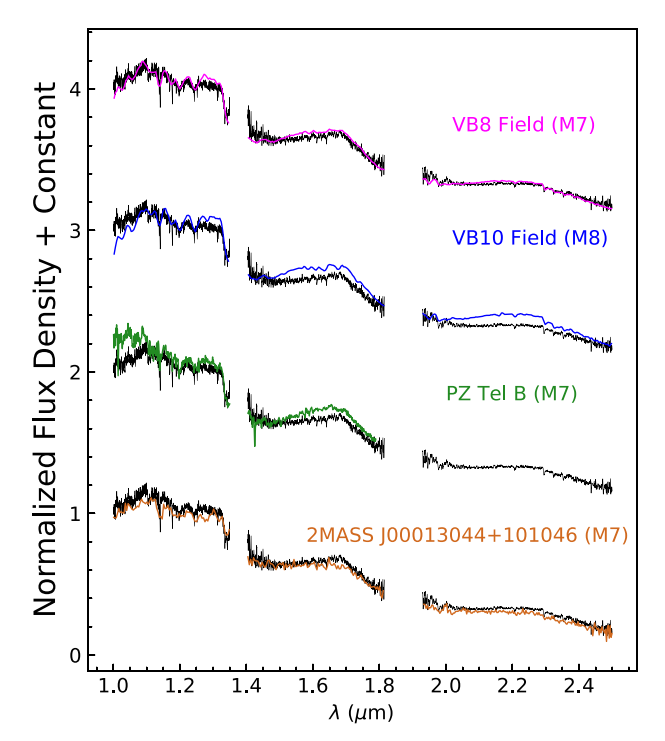


Figure 5. Comparison between our SpeX spectrum of 2M0443+3723 B (black) and both young and field ultracool dwarfs. The best-fitting spectrum from the χ^2_{ν} comparison with M, L, and T dwarfs from the SpeX Prism Library is shown in orange (2MASS J0013044+1010146; Burgasser et al. 2004), while comparison to the young BD PZ Tel B (Maire et al. 2016) is displayed green. A field M7 dwarf (VB 8; Burgasser et al. 2008) and field M8 dwarf (VB 10; Burgasser 2014) are also plotted for comparison. 2M0443+3723 B is a close match to the VB 8 field M7 dwarf (Burgasser et al. 2008), as well as the young M7 dwarf 2MASS J00013044+101046.

objects with the following designations: 0 for field gravity dwarfs (FLD-G; $\gtrsim 200$ Myr), 1 for intermediate-age gravity dwarfs (INT-G; ~ 50 –200 Myr), and 2 for young low-gravity dwarfs (VL-G; ~ 10 –30 Myr). The final gravity score measured is 2 for 2M0443+3723 B, although individual gravity scores from the FeH_z and K I_J yield values of 1, corresponding to INT-G (Figure 6). Gravity scores have been shown to correlate with age (e.g., Liu et al. 2016); most VL-G objects are young (< 30 Myr).

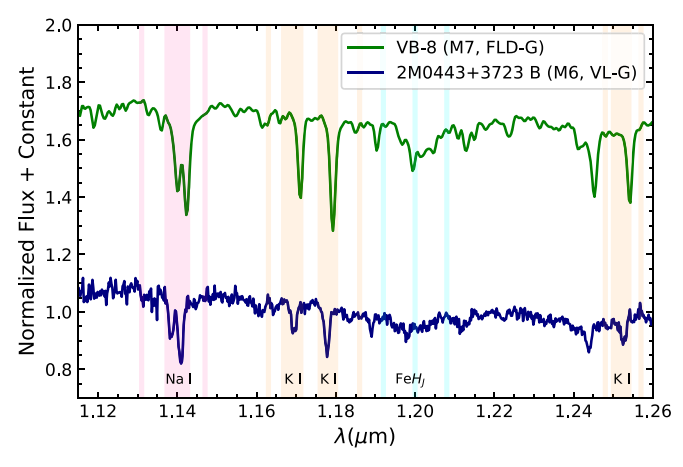


Figure 6. Our *J*-band IRTF/SpeX spectrum of 2M0443+3723 B (blue) compared to an FLD-G standard from the IRTF Spectral Library, VB 8 (green; Cushing et al. 2005). The Na I, K I, and FeH features of our companion are weaker than the FLD-G object, which indicates that 2M0443+3723 B is a young, low-gravity object. Note that the spectrum of VB 8 ($R \sim 2000$) has been smoothed to a resolution comparable to our SXD spectrum.

3.3. Atmospheric Properties of 2M0443+3723 B

We utilize the BT-Settl "CIFIST 2011–2015" grids⁶ (Allard et al. 2012) to determine the effective temperature and surface gravity of 2M0443+3723 B. These models span an effective temperature range of 1200–7000 K, with increments of 100 K, and surface gravities from 2.5–5.5 dex in increments of 0.5 dex. The models assume solar metallicity and do not include alpha-enhancement.

Our SXD data cover the entire NIR (0.7–2.4 μ m) range. We remove the low-S/N regions spanning the 1.4 and 1.9 μ m water bands of our medium-resolution spectrum, which are not used in the analysis. Each synthetic spectrum was smoothed to the resolving power of our medium-resolution SXD spectrum ($R \sim 750$) through convolution with a 1D Gaussian kernel. We normalize the synthetic spectra and our SXD spectrum at a common wavelength, resample the model grids to a common wavelength grid, and then optimally scale them to the flux-calibrated SXD spectrum by minimizing the χ^2 value between the model and data. We select the best-fitting physical parameters by locating the minimum χ^2 value from our SXD (Figure 7) spectral fit. For our SXD spectrum we find the best fit to be $T_{\rm eff} = 2800 \pm 100$ K and log $g = 4.0 \pm 0.5$ dex (Figure 8 and Table 1).

We use the *H*-band region (1.550–1.72 μ m) from our higher-resolution IGRINS ($R \sim 45{,}000$) spectrum of 2M0443+3723 B for our model fits. This portion of the *H*-band spectrum comprises 14 separate orders and contains the temperature-sensitive Al and Fe lines. We fit the model grids to each separate order to determine the temperature and gravity and then adopt the average values across 14 orders. We select the best-fitting physical parameters by locating the minimum χ^2 value from our IGRINS spectral fit (Figure 9). The best-fitting parameters from the IGRINS *H*-band region fit are $T_{\rm eff} = 2900 \pm 100$ K and $\log g = 4.5 \pm 0.5$ dex for the 1.55–1.72 μ m region.

The SpeX and IGRINS spectra both produce similar parameters from the model fits within 1σ error from each other.

http://perso.ens-lyon.fr/france.allard/

⁷ We employ the *H*-band IGRINS spectrum because it has more temperature-sensitive lines (Fe and Al), which are not degenerate with gravity like those in the *K* band (López-Valdivia et al. 2019).

Table 1
Summary of the Best-fitting Parameters Found from Our Fits of the Near-infrared Spectra of 2M0443+3723 B Using the BT-Settl "CIFIST 2011–2015" Grids

Object	Telescope/ Instrument	Region	T _{eff} (K)	log(g) (dex)	$\chi^2_{ u}$	χ^2
2M0443+3723 B	IRTF/SpeX (SXD)	0.68–2.4 μm	2800	4.0	0.016	37.35
2M0443+3723 B	DCT/IGRINS	1.550–1.72 μm	2900	4.5	0.052	

Note. Results from fitting the BT-Settl "CIFIST 2011–2015" atmospheric model grids to 2M0443+3723 B. The best solutions are shown for each of the regions used. Note that the χ^2 for the SpeX fit is 37.35, which produces best-fit parameters of $T_{\text{eff}} = 2800$ K and $\log g = 4.0$ dex.

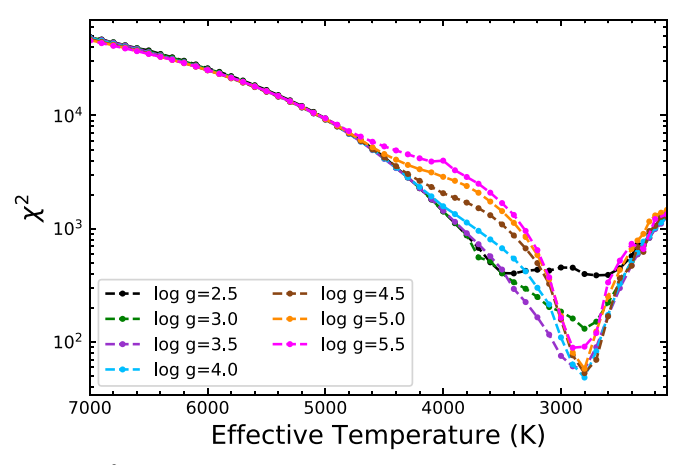


Figure 7. χ^2 values for fits to our SXD spectrum values across the effective temperature range of the BT-Settl "CIFIST 2011–2015" model grid. There is a convergence to a minimum at a temperature of 2800 K and log g of 4.0 dex.

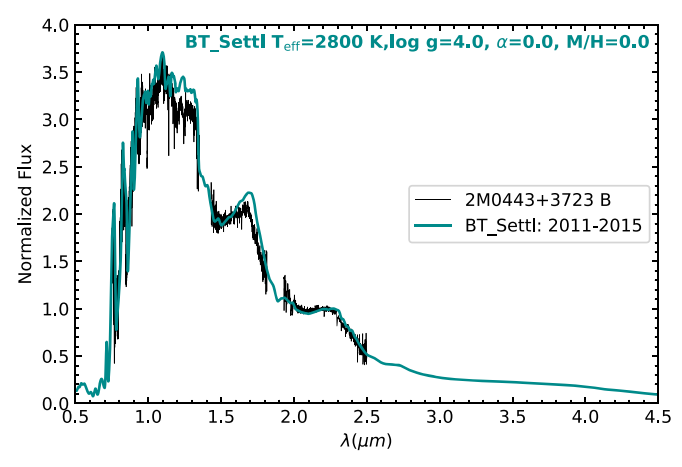


Figure 8. 2M0443+3723 B (black) SED compared to the best-fitting spectrum from the BT-Settl "CIFIST 2011–2015" atmospheric models.

The IRTF/SpeX spectrum samples a wider spectral grasp (the entire NIR region) compared to the H-band IGRINS spectrum, so we adopt those best-fitting parameters for this study.

3.4. Bolometric Luminosity

The bolometric luminosity of 2M0443+3723 B is derived using the BT-Settl atmospheric models (Allard et al. 2012) for bolometric corrections at short wavelengths ($\lambda < 0.68~\mu m$) and long wavelengths (2.4–500 μm). We flux-calibrate the $T_{\rm eff}=2800~{\rm K}$ and log g=4.0 dex BT-Settl model using the Two Micron All Sky Survey (2MASS) H-band apparent magnitude of 2M0443+3723 B and scale the synthetic spectrum to the data

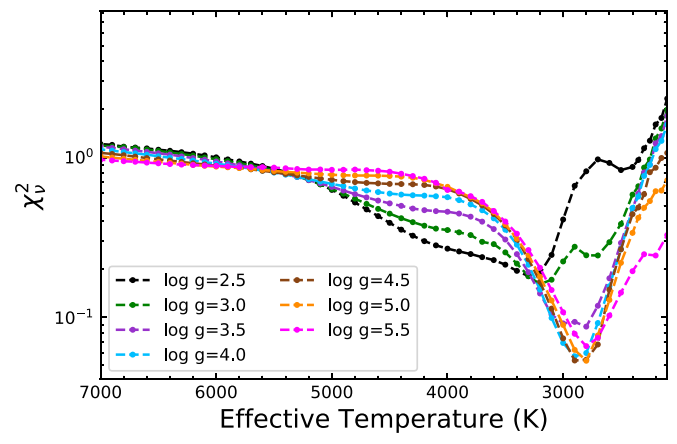


Figure 9. χ^2_{ν} values for fits to our IGRINS *H*-band spectrum values across the effective temperature range of the BT-Settl "CIFIST 2011–2015" model grid. There is a convergence to a minimum at a temperature of 2900 K and log *g* of 4.5 dex

using the optimal scaling factor (C_H) following Cushing et al. (2008):

$$C_H = 10^{-0.4m_H} \frac{\int \lambda f_{\lambda}^{\text{Vega}} T_H(\lambda) d\lambda}{\int \lambda f_{\lambda}^{\text{obs}}(\lambda) T_H(\lambda) d\lambda}.$$
 (2)

Here $T_H(\lambda)$ is the transmission profile of the 2MASS H band, $f_{\lambda}^{\text{Vega}}$ is the flux density for Vega, λ is the wavelength array for 2M0443+3723 B, f_{λ}^{obs} is the flux density of the science target, and m_H is the 2M0443+3723 B H-band magnitude from 2MASS.

The bolometric luminosity is then

$$L_{bol} = 4\pi d^2 \int_{0.125 \mu m}^{500 \mu m} F_{\lambda} d\lambda,$$

where F_{λ} is the flux-calibrated spectrum and d represents the distance to 2M0443+3723 B. The bolometric flux we find for 2M0443+3723 B is 4.17×10^{-14} W m⁻². We utilize a Monte Carlo method to calculate the bolometric luminosity by taking into account the uncertainties from the 2MASS H-band photometry, measurement errors from our SXD spectrum of 2M0443+3723 B, and the distance. A distance of 72.4 ± 0.8 pc is used from the Gaia DR2 parallax measurement for 2M0443+3723 B. This yields a bolometric luminosity of $L_{\rm bol} = -2.16 \pm 0.02$ dex.

3.5. Mass

Mass is a fundamental property used to distinguish BDs from gas giants and low-mass stars. Evolutionary models are generally necessary to infer masses using bolometric luminosities and ages of substellar objects (e.g., Burrows et al. 2001). Assuming membership in the β MPG (see Section 4.1), we adopt an age of 23 \pm 3 Myr (Mamajek & Bell 2014) for 2M0443+3723 B. The mass is then determined following a Monte Carlo approach with 10^6 trials using the bolometric luminosity and age for 2M0443 +3723 B. The median and standard deviation of this mass distribution is 99 ± 5 $M_{\rm Jup}$ if 2M0443+3723 B is single. We also derived the mass for scenarios in which this companion is not single (Section 4.4) or is not a member of the β PMG (Section 4.1). We find a mass of 52 ± 3 $M_{\rm Jup}$ if it is an equalflux binary and 30–110 $M_{\rm Jup}$ if it is a single young field object ($\lesssim 30$ Myr).

3.6. Radial Velocities

We measure RVs of 2M0443+3723 A and 2M0443+3723 B following Mann et al. (2016). We cross-correlate >250 order segments of the IGRINS ($R \sim 45,000$) H- and K-band spectra. For each segment we cross-correlate the telluric spectrum to find offsets in the wavelength solution between epochs of observation, and the target spectrum pixel offset was converted into an RV using the instrument dispersion solution. The measured RV is the median of the >250 segment measurements compared with >150 M2-M6 templates with known RVs. Our reported RV was barycenter corrected and shifted to the absolute scale using the RVs of the M2-M6 templates. Uncertainties in the RVs are the standard deviation of the mean added in quadrature with the absolute scale zero-point uncertainty of $\sim 150 \text{ m s}^{-1}$. For 2M0443+3723 A we find an RV_A = 7.0 \pm 0.2 km s⁻¹. For 2M0443+3723 B we find an RV_B = 5.8 \pm 0.2 km s⁻¹. These values are smallar to previous measurements of the host star, 2M0443+3723 A: the RV of 2M0443+3723 A has been measured to be $6.0 \pm 2.0 \, \mathrm{km \, s}^$ from Schlieder et al. (2010) and $6.4 \pm 0.3 \,\mathrm{km \, s}^{-1}$ from Shkolnik et al. (2017).

3.7. Radius

The radii of BDs can provide additional evidence of youth. During the course of their lifetimes, BDs continuously contract as they dissipate their leftover energy from formation. As BDs age, their radii eventually settle at $\sim 1\,R_{\rm Jup}$ as degeneracy pressure sets in. As a result, an inflated radius can serve as a youth indicator (Filippazzo et al. 2015).

We previously determined an effective temperature of $2800 \pm 100 \, \text{K}$ from atmospheric models and a bolometric flux (F_{Bol}) from integrating our flux-calibrated spectrum. We also have a precise measured distance from Gaia DR2. The Stefan-Boltzmann law can be used to determine the radius of 2M0443 $+3723 \, \text{B}$:

$$R = \left(\frac{F_{\text{Bol}}d^2}{\sigma T^4}\right)^{\frac{1}{2}}.$$

Radius uncertainties are computed using a Monte Carlo approach with the associated errors from the effective temperature, bolometric flux, and distance. We find an inflated radius $0.35 \pm 0.03~R_{\odot}$ (3.5 $R_{\rm Jup}$), an additional indication that 2M0443 +3723 B is young. For comparison, the old field object 2MASS J02530084+1652532 has a radius of $1.20 \pm 0.09~R_{\rm Jup}$ with a spectral type of M7 and $T_{\rm eff} = 2688 \pm 212~{\rm K}$ (Filippazzo et al. 2015).

4. Discussion

4.1. Moving Group Membership Assessment

BANYAN (Bayesian Analysis for Nearby Young AssociatioNs) Σ is a tool developed by Gagné et al. (2018) that analyzes galactic positions and space velocities to determine membership probabilities in nearby young associations. BANYAN Σ achieves a 90% recovery rate of known members if full kinematic parameters are provided. Gagné et al. (2018) use proper motions, RVs, parallaxes, and sky coordinates to determine the likelihood that an object belongs to any of the 27 associations spanning ages 1–800 Myr or the field population.

The 2M0443+3723 AB system has been proposed as a member of the β PMG in several studies (Schlieder et al. 2010; Malo et al. 2014; Shkolnik et al. 2017). Recently, Lee & Song (2019) developed BAMG (Bayesian Analysis of Moving Group), a four-stage moving group membership tool. This new tool lists 2M0443+3723 A as a highly likely member with a 86.2% membership probability for the β PMG. Yet BANYAN Σ yields a membership probability for 2M0443+3723 A of 0.4% for β PMG and 99.6% for the field. This discrepancy may be a result of restrictive kinematic and spatial priors from BANYAN Σ and/or the iterative membership approach used by Lee & Song (2019). For 2M0443+3723 B, BANYAN Σ gives 0.0% for the β PMG and 99.9% for the field.

Using updated astrometric and kinematic data from Gaia DR2, we determine the *XYZ* positions and *UVW* space motions of the pair along with uncertainties (Figure 10 and Table 2). The β PMG has average *XYZ* positions of *X*, *Y*, $Z_{\beta PMG} = \{4.1 \pm 29.3, -6.7 \pm 14.0, -15.7 \pm 9.0 \text{ pc}\}$ and space velocities *U*, *V*, $W_{\beta PMG} = \{-10.9 \pm 2.2, -16.0 \pm 0.3, -9.2 \pm 0.3 \text{ km s}^{-1}\}$ (Gagné et al. 2018).

We explored another quantitative approach to determine membership properties by comparing the 3D velocity difference between 2M0443+3723 AB and known YMGs using a reduced χ^2 metric following Shkolnik et al. (2012); see their Equation (14). This method allows for a membership examination that solely relies on galactic velocities and neglects XYZ parameters that can affect Bayesian methods if the prior is too restrictive. Here we adopt a cutoff value of $\chi^2_{\nu, \text{UVW}} \leqslant 4$ for consideration. A visualization of this method is shown in Figure 11. For each group we calculate the following two goodness-of-fit metrics:

$$\tilde{\chi}_{\text{UVW}}^2 = \frac{1}{3} \left[\frac{(U_{\star} - U_{\text{MG}})^2}{(\sigma_{U_{\star}}^2 + \sigma_{U,MG}^2)} + \frac{(V_{\star} - V_{\text{MG}})^2}{(\sigma_{V_{\star}}^2 + \sigma_{V,MG}^2)} + \frac{(W_{\star} - W_{\text{MG}})^2}{(\sigma_{W_{\star}}^2 + \sigma_{W,MG}^2)} \right]$$
(3)

$$\tilde{\chi}_{XYZ}^{2} = \frac{1}{3} \left[\frac{(X_{\star} - X_{MG})^{2}}{(\sigma_{X_{\star}}^{2} + \sigma_{X,MG}^{2})} + \frac{(Y_{\star} - Y_{MG})^{2}}{(\sigma_{Y_{\star}}^{2} + \sigma_{Y,MG}^{2})} + \frac{(Z_{\star} - Z_{MG})^{2}}{(\sigma_{Z_{\star}}^{2} + \sigma_{Z,MG}^{2})} \right]. \tag{4}$$

Here the subscript \star represents the values for the object in question and the subscript MG represents a selected moving group. Shkolnik et al. (2012) assumed a constant velocity dispersion (σ) of $2 \,\mathrm{km \, s^{-1}}$ for the *UVW* motions to avoid biasing their results in favor of moving groups with larger

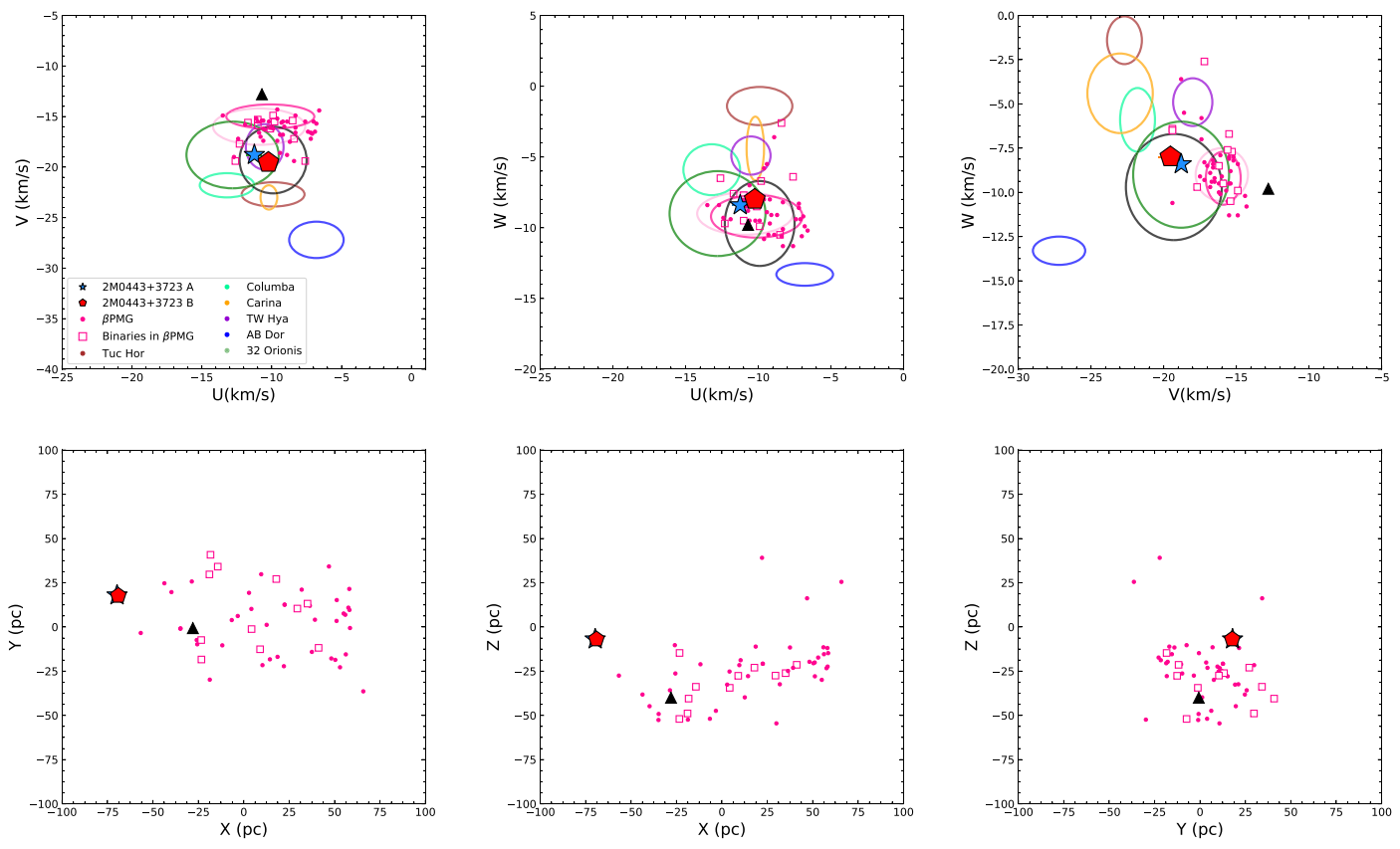


Figure 10. *UVW* galactic space velocities and *XYZ* heliocentric positions of 2M0443+3723 A and 2M0443+3723 B (blue star and red pentagon, respectively) and those of nearby YMGs. The 3σ dispersion in *UVW* velocities for the βPMG from Torres et al. (2008) is shown with dark pink circles, and that from Gagné et al. (2018) is shown in light pink for comparison. βPMG members are from Shkolnik et al. (2017). These are the available M dwarf members with confirmed membership in this group (pink circles). Those designated with an "N" or "Y?" from that study have been excluded. Binaries from the βPMG are shown as pink squares, and the substellar companion, 2MASS J0249–0557c, is shown as a black triangle. Ellipses represent the 3σ confidence limits of the moving groups. βPMG members are generally clustered together in *UVW* space but are dispersed over many tens of parsecs as shown in the *XYZ* galactic position plots. If 2M0443+3723 AB is a member of this group, then it is a kinematic and spatial outlier relative to the current population.

velocity dispersions. Here we use the locus and dispersion for each of the 27 associations included in Gagné et al. (2018) in this analysis.

Twelve associations have $\chi^2_{\nu, \rm UVW} \leqslant 4$: 118TAU, $\beta \rm PMG$, EPSC, ETAC, LCC, TAU, THOR, TWA, UCL, UCRA, USCO, and XFOR. Nearly all of these have inconsistent distances or sky positions relative to 2M0443+3723 AB (Figure 12). 2M0443+3723 A has the best match to the THOR (32 Orionis) association ($\chi^2_{\nu, \rm UVW} = 0.6$). THOR has an age of ~22 Myr (Bell et al. 2015) and a typical distance of 96 \pm 2 pc. This disagrees with the Gaia parallactic distance of 72.4 \pm 0.8 pc. The EPSC (ϵ Chamaeleontis) group has an average age of ~3.7 Myr (Murphy et al. 2013) and lies at an average distance of 102 ± 4 pc primarily in the southern hemisphere. This distance excludes EPSC even though this group has the lowest $\chi^2_{\nu, \rm UVW}$ for 2M0443+3723 B ($\chi^2_{\nu, \rm UVW} = 0.26$). TAU (Taurus) is a ~1–2 Myr (Kenyon & Hartmann 1995) star-

TAU (Taurus) is a \sim 1–2 Myr (Kenyon & Hartmann 1995) star-forming region; its members lie at an average distance of 120 \pm 10 pc, which makes it too distant to host the 2M0443+3723 AB system. 118 Tau is a young \sim 10 Myr association located at an average distance of 145 \pm 15 pc (Galli et al. 2018), which is likewise inconsistent with the distance of 2M0443+3723 AB (72.4 \pm 0.8 pc). TWA (TW Hya) has a younger age of \sim 10 Myr (Bell et al. 2015). This system would be a probable match for 2M0443+3723 AB given the distance distribution (60 \pm 10 pc), but its members are tightly clustered in the southern hemisphere.

At \sim 500 Myr (Pöhnl & Paunzen 2010), XFOR is one of the oldest associations located at an average distance of 100 \pm 6 pc. Similarly, UCRA and ETAC are located too far south. The Sco-Cen star-forming region hosts UCL, LCC, and USCO; it can collectively be eliminated owing to the distances of \sim 110–154 pc.

The velocity modulus (Equation (5)) can also be calculated to further assess membership probabilities for nearby YMGs:

$$\Delta \nu = \sqrt{(U_{\star} - U_{\rm MG})^2 + (V_{\star} - V_{\rm MG})^2 + (W_{\star} - W_{\rm MG})^2}.$$
 (5)

The advantage of this metric is that it accounts for moving groups with large UVW velocity dispersions by just focusing on the velocity locus. We adopt a cutoff $\Delta\nu$ of $5~{\rm km~s}^{-1}$ (following Shkolnik et al. 2012; Figure 13). Ten associations have $\Delta\nu\leqslant 5~{\rm km~s}^{-1}$: 118TAU, $\beta{\rm PMG}$, CAR, COL, EPSC, ETAC, LCC, THOR, TWA, and XFOR. As previously discussed, most of these associations are not a good match owing to discrepancies with their distances declinations (Figure 12).

For the β PMG, $\chi^2_{\nu, \rm UVW}=3.13$ for 2M0443+3723 B and $\chi^2_{\nu, \rm UVW}=1.92$ for 2M0443+3723 A. The $\chi^2_{\nu, \rm XYZ}$ values for 2M0443+3723 B and 2M0443+3723 A are 3.72 and 2.87, respectively. The β PMG does not have the lowest $\chi^2_{\nu, \rm UVW}$, but we conclude that it is the most probable moving group to host 2M0443+3723 AB. Similarly, $\chi^2_{\nu, \rm XYZ}$ and $\Delta \nu$ values for 2M0443+3723 AB indicate that the β PMG is the most likely of the known moving groups to host 2M0443+3723 AB.

Table 2Properties of the 2M0443+3723 AB System

Property	2M0443+3723 A	2M0443+3723 B	References
	Positions and		
	Kinematics		
R.A. (deg)	70.98707	70.98975	6
Decl. (deg)	37.38400	37.38394	6
Parallax (mas)	13.9572 ± 0.0518	13.8198 ± 0.1585	6
Distance (pc) ^a	71.6 ± 0.3	72.4 ± 0.8	1
$\mu_{\alpha} \cos \delta$ (mas ${\rm yr}^{-1}$)	22.869 ± 0.097	24.204 ± 0.261	6
μ_{δ} (mas yr ⁻¹)	-61.837 ± 0.060	-61.670 ± 0.156	6
$RV (km s^{-1})$	7.0 ± 0.2	5.8 ± 0.2	1
vsini (kms ⁻¹)	13.3 ± 0.8	15.2 ± 0.8	1
X (pc)	-69.07 ± 0.25	-69.75 ± 0.84	1
Y (pc)	17.72 ± 0.08	17.89 ± 0.24	1
Z (pc)	-6.92 ± 0.05	-6.98 ± 0.15	1
$U (\mathrm{km \ s}^{-1})$	-11.25 ± 0.19	-10.23 ± 0.20	1
$V (\text{km s}^{-1})$	-18.79 ± 0.09	-19.53 ± 0.24	1
W (km s ⁻¹)	-8.41 ± 0.04	-7.98 ± 0.121	1
	Photometry		
$J_{2\text{MASS}}$ (mag)	9.71 ± 0.02	12.22 ± 0.03	2
$H_{2\text{MASS}}$ (mag)	9.03 ± 0.02	11.80 ± 0.04	2
$K_{S,2MASS}$ (mag)	8.80 ± 0.02	11.46 ± 0.03	2
B (mag)	15.35	•••	10
V (mag)	13.3 ± 0.09	•••	9
G_{Gaia} (mag)	12.327 ± 0.002	16.160 ± 0.001	6
g (mag)	14.00 ± 0.09		9
r (mag)	12.68 ± 0.06		9
i (mag)	11.56 ± 0.12		9
W1 (mag)	8.66 ± 0.02	11.92 ± 0.07	3
W2 (mag)	8.56 ± 0.02	10.93 ± 0.05	3
W3 (mag)	8.35 ± 0.02	10.56 ± 0.13	3
W4 (mag)	7.551 ± 0.16	8.191	3
$M_{J, 2MASS}$ (mag)	5.41 ± 0.03	7.92 ± 0.03	1
$M_{H,2\text{MASS}}$ (mag)	4.73 ± 0.003	7.50 ± 0.04	1
$M_{K,2\text{MASS}}$ (mag)	4.502 ± 0.04	7.16 ± 0.03	1
J–H (mag)	0.68	0.42	1
H– K (mag)	0.228	0.35	1
J–K (mag)	0.908	0.77	1
	Fundamental Properties		
$\log(\frac{L_{bol}}{L_{\odot}})(\text{dex})$	0.73 ± 0.02	-2.16 ± 0.02	4,1
Spectral Type	$M2 \pm 1$	$M6 \pm 1$	5,1
Mass $(M_{Jup})^{b}$		99 ± 5	1
Age (Myr) ^b	23 ± 3	23 ± 3	7
$T_{\rm eff}$ (K)	3700	2800 ± 100	8,1
$\log g \text{ (dex)}$	5.0	4.0 ± 0.5	8,1
105 g (uca)	5.0	T.O 0.3	0,1

Notes.

Separation

(arcsec)

Radius (R_{\odot})

Separation (AU)

7.46

550

 $0.35\,\pm\,0.03$

5

5

4,1

 0.68 ± 0.22

References. (1) This work; (2) 2MASS (Cutri et al. 2003); (3) WISE (Cutri et al. 2012); (4) Messina et al. (2017); (5) Schlieder et al. (2010); (6) Gaia (Gaia Collaboration et al. 2018); (7) Mamajek & Bell (2014); (8) Malo et al. (2014); (9) APASS (Zacharias et al. 2012); (10) Norton et al. (2007).

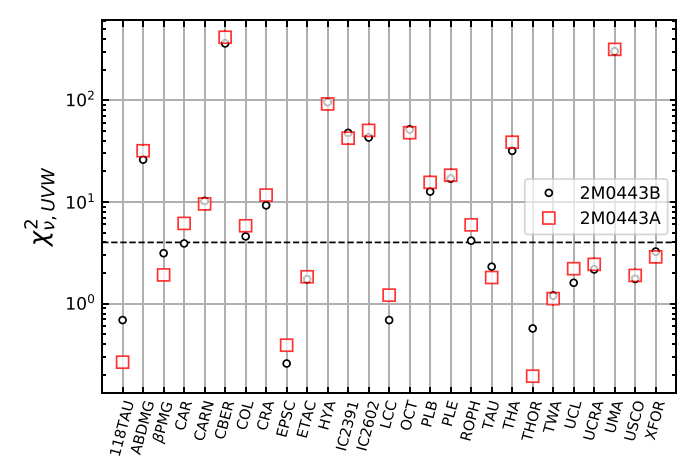


Figure 11. $\chi^2_{\nu,\rm UVW}$ values for 27 known groups used in BANYAN Σ (Gagné et al. 2018). The full names of young associations are 118 Tau (118TAU), AB Doradus (ABDMG), β Pictoris (β PMG), Carina (CAR), Carina-Near (CARN), Coma Berenices (CBER), Columba (COL), Corona Australis (CRA), ϵ Chamaeleontis (EPSC), η Chamaeleontis (ETAC), the Hyades (HYA), Lower Centaurus Crux (LCC), Octans (OCT), Platais 8 (PL8), Pleiades (PLE), ρ Ophiuchi (ROPH), the Tucana-Horologium association (THA), 32 Orionis (THOR), TW Hya (TWA), Upper Centaurus Lupus (UCL), Upper CrA (UCRA), the core of the Ursa Major cluster (UMA), Upper Scorpius (USCO), Taurus (TAU), and χ^1 For (XFOR). 2M0443+3723 B is shown as black circles, and 2M0443+3723 A is shown with red squares. Several groups are good UVW matches to 2M0443+3723 AB but disagree when distance and decl. are considered. Altogether, 2M0443+3723 AB is most consistent with the β PMG, although if it is a member it would be a kinematic outlier ($\Delta \nu = 3.7 \ {\rm km \ s}^{-1}$).

4.2. Comparison to Ultracool Companions in the β Pictoris Moving Group

Over 1000 isolated BDs are known, but BD companions are much rarer. The frequency of BDs that are companions to stars is 2%–4%; these occurrence rates are independent of stellar mass or spectral type (Bowler & Nielsen 2018). To date there have only been a handful of ultracool companions discovered in the β PMG (see Dupuy et al. 2018 Table 5): HR 7329 B (Lowrance et al. 2000), PZ Tel B (Biller et al. 2010; Mugrauer et al. 2010), β Pic b (Lagrange et al. 2010), 51 Eri b (Macintosh et al. 2015), and 2MASS J0249–0557c (Dupuy et al. 2018). The spectral types of these companions range from M7 to T6.5, and their masses span 11–72 $M_{\rm Jup}$. The spectral sequence of these objects is shown in Figure 14. In addition, the membership compilation by Shkolnik et al. (2017, their Table 4) lists one additional ultracool companion, the M6 object GJ 3076 B.

4.2.1. Planetary-mass Companions: 2MASS J0249–0557c, β Pic b, and 51 Eri b

There are currently three known planetary-mass companions in the β PMG: 2MASS J0249–0557c, β Pic b, and 51 Eri b. Here we provide a brief overview of each system.

2MASS J0249–0557c (Dupuy et al. 2018) has a spectral type of L2 \pm 1, a luminosity of log(L/L_{\odot}) = -4.00 ± 0.09 dex,

^a Bailer-Jones et al. (2018) find consistent values of 71.5 \pm 0.26 pc and 72.4 \pm 0.8 pc for 2M0443A and 2M0443B, respectively, using probabilistic inference from parallax measurements.

^b Masses and ages assume membership in the β PMG.

⁸ Note that both 2MASS J01365516–0647379 and 2MASS J08224744–5726530 are listed in Table 4 of Shkolnik et al. (2017) as having companions with spectral types >L0, but photometry from Janson et al. (2012) indicates that the companion to 2MASS J08224744–5726530 is ≈M5.5, and deep imaging of 2MASS J01365516–0647379 from Bowler et al. (2015) did not reveal any comoving companions.

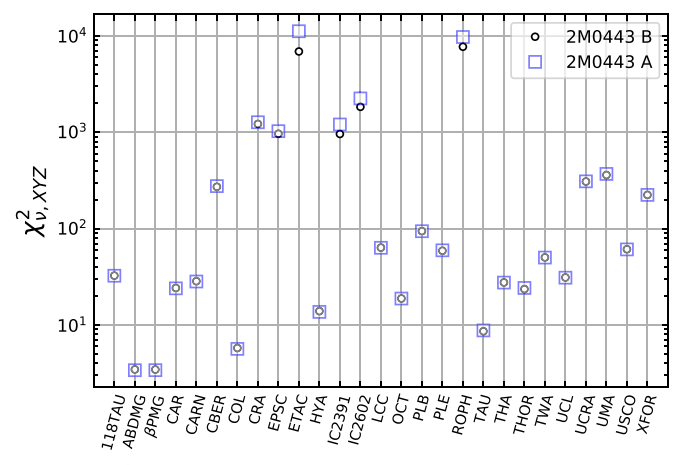


Figure 12. $\chi^2_{\nu,XYZ}$ values for 27 known groups used in BANYAN Σ. Groups names are the same as in Figure 11.

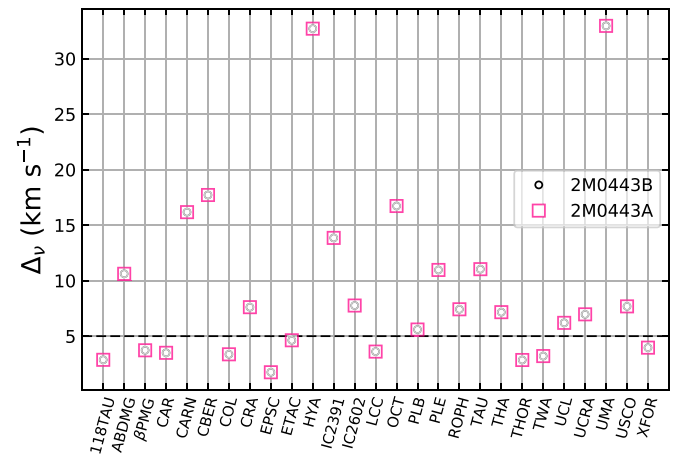


Figure 13. Velocity modulus of 27 known moving groups and associations. A cutoff value of 5 km s^{-1} is shown with a dotted line.

and an estimated mass of $11.6^{+1.3}_{-1.0}~M_{\rm Jup}$. It lies at a separation of 40" (1950 au) from its host, which is a tight equal-flux ratio BD binary with an integrated-light spectral type of M6 \pm 1.

51 Eri b (Macintosh et al. 2015) has a spectral type of T6.5 \pm 1.5, an estimated mass of 2–12 $M_{\rm Jup}$, and an effective temperature of 605–737 K. Rajan et al. (2017) report a bolometric luminosity of $-5.83^{+0.15}_{-0.12}$ to $-5.93^{+0.19}_{-0.14}$ dex. 51 Eri b orbits its massive F0IV host star at a separation of 0."45 (13.2 au).

 β Pic b (Lagrange et al. 2010) has a spectral type of L2 \pm 1 and orbits the namesake member of the β PMG, the A6V type star, β Pic, at a separation of 0."13 (9 au; Lagrange et al. 2019). Dupuy et al. (2019) find a model-independent dynamical mass of 13 \pm 3 $M_{\rm Jup}$, comparable to results from Snellen & Brown (2018). Chilcote et al. (2017) find an effective temperature of 1700 K and a bolometric luminosity of $\log(L/L_{\odot}) = -3.76 \pm 0.02$ dex.

4.2.2. Brown Dwarf Companions: HR 7329 B and PZ Tel B

HR 7329 B (Lowrance et al. 2000) was the first BD companion identified in the β PMG. It orbits at a separation of 4" (220 au) from its massive A0V host star, HR 7329 A. Bonnefoy et al. (2014) derive a spectral type of M8.5 \pm 0.5, with an effective temperature of 2200–2500 K, a luminosity of

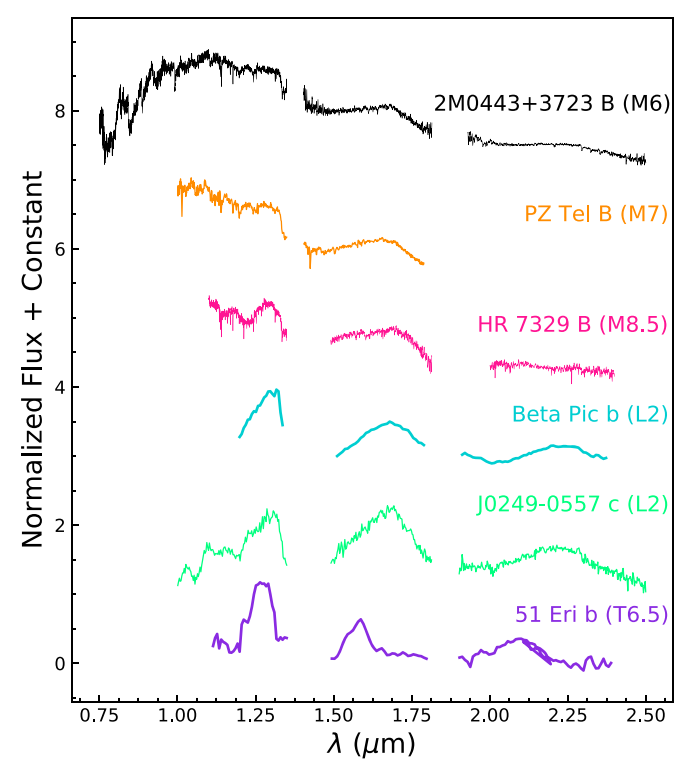


Figure 14. Spectral sequence of known substellar companions in the βPMG along with our medium-resolution SXD spectrum of the candidate benchmark BD, 2M0443+3723 B. PZ Tel B and HR 7329 B have masses above the deuterium-burning limit (\sim 13 $M_{\rm Jup}$), while J0249–0557c, β Pic b, and 51 Eri b have masses below the deuterium-burning limit (Lowrance et al. 2000, Biller et al. 2010; Lagrange et al. 2010, Mugrauer et al. 2010, Macintosh et al. 2015, Dupuy et al. 2018). Spectra of known substellar companions are from Bonnefoy et al. (2014), Maire et al. (2016), Chilcote et al. (2017), Dupuy et al. (2018), and Rajan et al. (2017).

 $\log(L/L_{\odot}) = -2.627 \pm 0.087$ dex, and a model-dependent mass of $\sim 20-50~M_{\rm Jup}$ (Neuhäuser et al. 2011).

The substellar companion PZ Tel B (Biller et al. 2010; Mugrauer et al. 2010) has a separation of 0."5 (\sim 25 au) from its G9IV host star. PZ Tel B has a spectral type of M7 \pm 1, an effective temperature of 2700 \pm 100 K, a luminosity of $\log(L/L_{\odot}) = -2.51 \pm 0.10$ dex, and a model-dependent mass of 59 $^{+13}_{-8}$ $M_{\rm Jup}$ —well within the BD mass regime (Maire et al. 2016).

4.3. Color-Magnitude Diagrams

In Figure 15, color–magnitude diagrams are used to compare the photometry of 2M0443+3723 B to ultracool objects in β PMG and the field. We combine the parallactic distance to 2M0443+3723 B from Gaia DR2 with 2MASS photometry to derive absolute magnitudes (Table 2).

2M0443+3723 B has a slightly bluer J-K color and is about 0.9 mag brighter in M_H than PZ Tel B. However, it is nearly identical to the M6 pair 2M0249-0557 A and B when using their parallactic distance as measured by Gaia.

4.4. Is 2M0443+3723 B a Close Binary?

The empirical analysis of 2M0443+3723 B implies a higher bolometric luminosity for a single object in β PMG compared to other M6–M7 members (Figure 16). This may mean that this

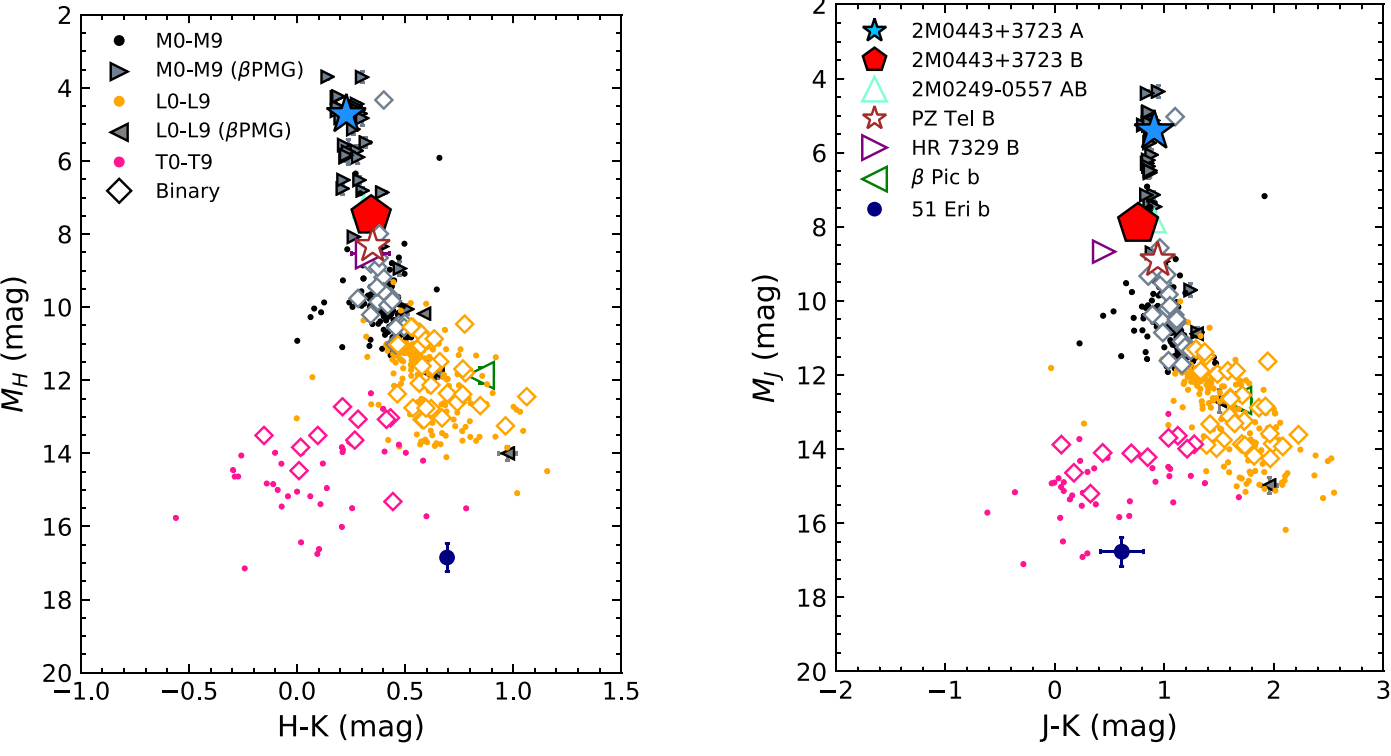


Figure 15. M_H vs. (H-K) (left) and M_J vs. (J-K) (right) color–magnitude diagrams of BDs and gas giants (M–T spectral types) from the βPMG and other field ultracool dwarfs compared to 2M0443+3723 B (red pentagon). 2M0443+3723 B is brighter than the other single BD companion, PZ Tel B (M7 ± 1). All photometry is on the 2MASS system. Photometry is shown for young M dwarfs from the βPMG (right-pointing blue triangles) and L dwarfs from the βPMG (left-pointing gray triangles). 2M0443+3723 A is shown with a blue star. Binaries are shown (diamonds) and substellar companions in the βPMG are labeled: PZ Tel B, HR 7329 B, β Pic b, and 51 Eri b. Photometries are from Dupuy & Liu (2012), Dupuy & Kraus (2013), Liu et al. (2016), and Dupuy et al. (2018).

companion is itself a close binary, or that it is not a member of the βPMG .

As described in Section 2.3, we acquired AO images with Keck II/NIRC2 to investigate the possibility that 2M0443 +3723 B is itself a close binary. After the basic image reduction, the dithered science frames were registered, shifted to the common centroid position of the companion, and median-combined to produce the co-added image of the companion shown in Figure 17. There are no obvious indications that 2M0443+3723 B is a close binary from these diffraction-limited images.

We carried out basic PSF "roll angle subtraction" to further assess whether 2M0443+3723 B is a close, marginally resolved binary. To mimic "roll subtraction" (Liu 2004; Song et al. 2006), the image of the companion was rotated and subtracted from the nonrotated reference image (Figure 17) to search for potential companions that could account for the abnormally high luminosity of 2M0443+3723 B, assuming membership in the β PMG. The same procedure was carried out for 36 equally spaced roll angles spanning 10°–350°. After performing PSF subtraction, we noted a point source adjacent to 2M0443+3723 B; however, this same source is visible in the image of 2M0443+3723 A, which indicates that this residual artifact is part of the speckle pattern and not a true companion (Figure 18).

We analyzed the IGRINS spectra of 2M0443+3723 A and 2M0443+3723 B to search for signs of spectroscopic binarity by utilizing a cross-correlation analysis of 2M0443+3723 A and 2M0443+3723 B against one another. This cross-correlation confirms the RV difference and shows no trace of a third component in the system. However, we cannot rule out

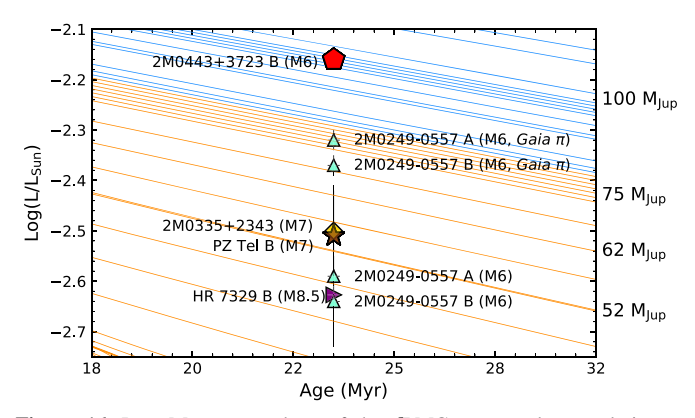


Figure 16. Late M-type members of the βPMG compared to evolutionary "isomass" model tracks from Burrows et al. (2001). The orange lines represent BDs, and the blue lines represent low-mass stars. Known BD companions in the βPMG are labeled and shown alongside 2M0443+3723 B (red pentagon). Note that we also include the 2M0249–0557 AB bolometric luminosity values found by Dupuy et al. (2018) using the Gaia DR2 parallax (aquamarine triangles) in addition to the values from the Hawaii Infrared Parallax Program. PZ Tel B (brown star) and HR 7329 B (purple triangle) are clearly within the BD regime, while 2M0443+3723 B lies near the hydrogen-burning limit, which is surprising if it is a single member of this group because it has a similar spectral type to 2M0249–0557 AB and PZ Tel B.

the presence of a significantly lower mass companion in this system.

5. Conclusions

We have presented a detailed characterization of 2M0443 +3723 B, a wide companion candidate BD to a lithium-rich M

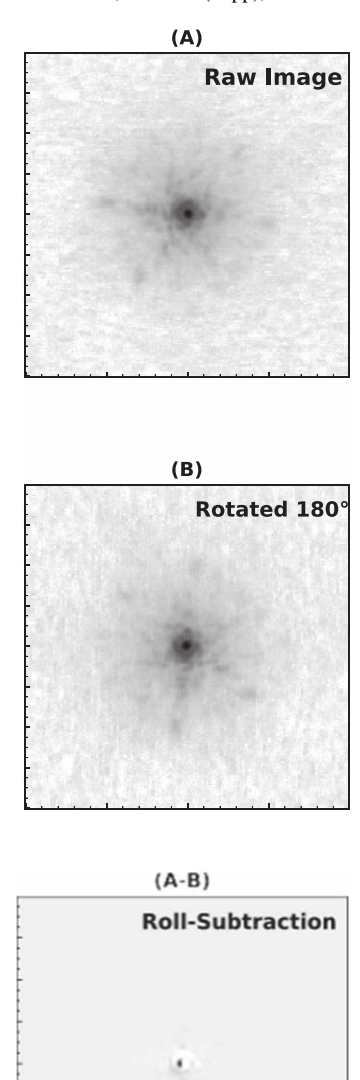
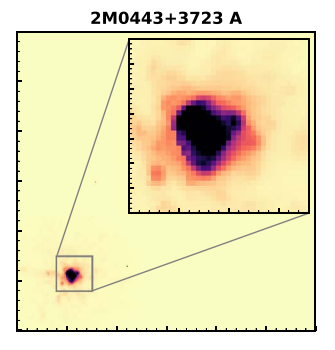


Figure 17. Steps involving classical "roll angle subtraction" PSF subtraction. Top: final median-combined 2" × 2" Keck II/NIRC2 image of 2M0443 +3723 B. Middle: roll subtraction method using a 180° roll angle. Bottom: difference between image A and B. A candidate companion is visible in the A–

B image, but this is likely a speckle because a similar feature is present in the

dwarf that may belong to the β PMG. We obtained an NIR spectrum from IRFT/SpeX and find an M6 \pm 1 spectral type and VL-G gravity classification using the index-based system of Allers & Liu (2013). 2M0443+3723 B has an inflated radius of 3.5 $R_{\rm Jup}$, and BT-Settl atmospheric model fits yield $T_{\rm eff}=2800\pm100\,{\rm K}$ and log $g=4.0\pm0.5$ dex. We also calculate a bolometric luminosity of -2.16 ± 0.02 dex. This luminosity combined with the age of the β PMG, 23 \pm 3 Myr (Mamajek & Bell 2014), implies a model-dependent mass of 99 \pm 5 $M_{\rm Jup}$. This mass and luminosity are higher than those of other M6 members of the β PMG.

We acquired AO images with Keck II/NIRC2 to explore the possibility that the companion could be a close binary, which could explain this anomalously high luminosity and corresponding



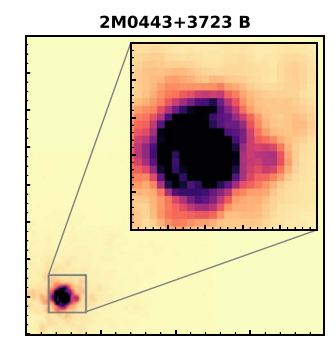


Figure 18. Visual inspection of the point source resembling a close companion to 2M0443+3723 B. Right: magnified image of the host star, 2M0443+3723 B in a $3'' \times 3''$ cutout. Left: magnified median-combined Keck II/NIRC2 image 2M0443+3723 A in a $2'' \times 2''$ cutout. The point source is present near 2M0443+3723 B and 2M0443+3723 A. This indicates that the source is part of the speckle pattern and not a companion.

higher mass. PSF subtraction does not reveal any close, modest flux ratio point sources. We reassess whether the 2M0443+3723 AB system is a member of the β PMG as has been proposed in past studies (Schlieder et al. 2010; Malo et al. 2014; Shkolnik et al. 2017; Lee & Song 2019). We utilize the membership analysis tool BANYAN Σ (Gagné et al. 2018) and find low probability of membership in the β PMG of 0.0% and 0.4% for 2M0443+3723 B and 2M0443+3723 A, respectively. This is contrary to the 86.2% membership probability in the β PMG for 2M0443+3723 A found by Lee & Song (2019) using their BAMG membership analysis tool. We explored other analytical methods to evaluate membership and found the β PMG to be the most likely YMG, should this system belong to a known association, although it may also be a young field object.

Regardless of its status in the β PMG, 2M0443+3723 B is certainly young, and likely \lesssim 30 Myr. Our analysis shows that this system has various indicators of youth: an inflated radius for 2M0443+3723 B, lithium in the host, and VL-G classification. We expect the status of this system to be clarified as the spatial and kinematic distributions of the β PMG continue to be refined with parallaxes from Gaia and additional RVs of candidate members in the future.

We thank the anonymous referee for their time providing helpful comments that improved the quality of this paper. The authors wish to thank Michael Bonnefoy, Trent Dupuy, Abhijith Rajan, and Jeffrey Chilcote for providing spectra that were used in this work. The Database of Ultracool Parallaxes is maintained by Trent Dupuy. This research has benefited from the SpeX Prism Library (and/or SpeX Prism Library Analysis Toolkit), maintained by Adam Burgasser at http://www.browndwarfs.org/spexprism.

This work was supported by a NASA Keck PI Data Award, administered by the NASA Exoplanet Science Institute. Data presented herein were obtained at the W. M. Keck Observatory from telescope time allocated to the National Aeronautics and Space Administration through the agencies scientific partnership with the California Institute of Technology and the University of California. The Observatory was made possible by the generous financial support of the W. M. Keck Foundation. The authors wish to recognize and acknowledge the very significant cultural role and reverence that the summit of Maunakea has always had within the indigenous Hawaiian community. We are most fortunate to have the opportunity to conduct observations from

this mountain. We utilized data acquired with the SpeX instrument at the IRTF, which is operated by the University of Hawaii under contract NNH14CK55B with the National Aeronautics and Space Administration.

This work used the Immersion Grating Infrared Spectrometer (IGRINS) that was developed under a collaboration between the University of Texas at Austin and the Korea Astronomy and Space Science Institute (KASI) with the financial support of the US National Science Foundation under grant AST-1229522, of the University of Texas at Austin, and of the Korean GMT Project of KASI. These results made use of the Discovery Channel Telescope at Lowell Observatory. Lowell is a private, nonprofit institution dedicated to astrophysical research and public appreciation of astronomy and operates the DCT in partnership with Boston University, the University of Maryland, the University of Toledo, Northern Arizona University, and Yale University.

This publication makes use of data products from the Two Micron All Sky Survey, which is a joint project of the University of Massachusetts and the Infrared Processing and Analysis Center/California Institute of Technology, funded by the National Aeronautics and Space Administration and the National Science Foundation.

NASA's Astrophysics Data System Bibliographic Services, together with the VizieR catalog access tool and SIMBAD database operated at CDS, Strasbourg, France, were invaluable resources for this work.

This work has made use of data from the European Space Agency (ESA) mission Gaia (https://www.cosmos.esa.int/gaia), processed by the Gaia Data Processing and Analysis Consortium (DPAC, https://www.cosmos.esa.int/web/gaia/dpac/consortium). Funding for the DPAC has been provided by national institutions, in particular the institutions participating in the Gaia Multilateral Agreement.

B.P.B. acknowledges support from the National Science Foundation grant AST-1909209.

C.L.P. thanks the LSSTC Data Science Fellowship Program, which is funded by LSSTC, NSF Cybertraining grant No. 1829740, the Brinson Foundation, and the Moore Foundation; her participation in the program has benefited this work.

Facilities: Keck:II (NIRC2), IRTF (SpeX) DCT (IGRINS). Software: IGRINS Pipeline (Lee 2015), SpeXTool (Vacca et al. 2003; Cushing et al. 2004), cosmics.py package (van Dokkum 2001), BANYAN Σ (Gagné et al. 2018).

ORCID iDs

Caprice L. Phillips https://orcid.org/0000-0001-5610-5328
Brendan P. Bowler https://orcid.org/0000-0003-2649-2288
Gregory Mace https://orcid.org/0000-0001-7875-6391
Michael C. Liu https://orcid.org/0000-0003-2232-7664
Kimberly Sokal https://orcid.org/0000-0002-3621-1155

References

```
Allard, F., Homeier, D., & Freytag, B. 2012, RSPTA, 370, 2765
Allers, K. N., & Liu, M. C. 2013, ApJ, 772, 79
Bailer-Jones, C. A. L., Rybizki, J., Fouesneau, M., Mantelet, G., & Andrae, R. 2018, AJ, 156, 58
Basri, G., Marcy, G. W., & Graham, J. R. 1996, ApJ, 458, 600
Bell, C. P. M., Mamajek, E. E., & Naylor, T. 2015, MNRAS, 454, 593
Bell, C. P. M., Murphy, S. J., & Mamajek, E. E. 2017, MNRAS, 468, 1198
Beuzit, J.-L., Feldt, M., Dohlen, K., et al. 2008, Proc. SPIE, 7014, 701418
Biller, B. A., Liu, M. C., Wahhaj, Z., et al. 2010, ApJL, 720, L82
Biller, B. A., Liu, M. C., Wahhaj, Z., et al. 2013, ApJ, 777, 160
```

```
Bonnefoy, M., Chauvin, G., Lagrange, A.-M., et al. 2014, A&A, 562, A127
Bowler, B. P. 2016, PASP, 128, 102001
Bowler, B. P., Hinkley, S., Ziegler, C., et al. 2019, ApJ, 877, 60
Bowler, B. P., Liu, M. C., & Cushing, M. C. 2009, ApJ, 706, 1114
Bowler, B. P., Liu, M. C., Shkolnik, E. L., & Tamura, M. 2015, ApJS, 216, 7
Bowler, B. P., & Nielsen, E. L. 2018, in Handbook of Exoplanets, ed.
   H. Deeg & J. Belmonte (Cham: Springer), 155
Brandt, T. D., Dupuy, T. J., & Bowler, B. P. 2019, AJ, 158, 140
Burgasser, A. J. 2014, ASInC, 11, 7
Burgasser, A. J., Liu, M. C., Ireland, M. J., Cruz, K. L., & Dupuy, T. J. 2008,
    ApJ, 681, 579
Burgasser, A. J., McElwain, M. W., Kirkpatrick, J. D., et al. 2004, AJ,
   127, 2856
Burrows, A., Hubbard, W. B., Lunine, J. I., & Liebert, J. 2001, RvMP, 73, 719
Chilcote, J., Pueyo, L., de Rosa, R. J., et al. 2017, AJ, 153, 182
Chun, M., Toomey, D., Wahhaj, Z., et al. 2008, Proc. SPIE, 7015, 70151V
Crepp, J. R., Johnson, J. A., Fischer, D. A., et al. 2012, ApJ, 751, 97
Cushing, M. C., Marley, M. S., Saumon, D., et al. 2008, ApJ, 678, 1372
Cushing, M. C., Rayner, J. T., & Vacca, W. D. 2005, ApJ, 623, 1115
Cushing, M. C., Vacca, W. D., & Rayner, J. T. 2004, PASP, 116, 362
Cutri, R. M., Skrutskie, M. F., van Dyk, S., et al. 2003, The IRSA 2MASS All-
   Sky Point Source Catalog, NASA/IPAC Infrared Science Archive, http://
   irsa.ipac.caltech.edu/applications/Gator/
Cutri, R. M., Wright, E. L., Conrow, T., et al. 2012, Explanatory Supplement to
   the WISE All-Sky Data Release Products, http://wise2.ipac.caltech.edu/
   docs/release/allsky/expsup/index.html
David, T. J., Stauffer, J., Hillenbrand, L. A., et al. 2015, ApJ, 814, 62
Dupuy, T. J., Brandt, T. D., Kratter, K. M., & Bowler, B. P. 2019, ApJL,
Dupuy, T. J., & Kraus, A. L. 2013, Sci, 341, 1492
Dupuy, T. J., & Liu, M. C. 2012, ApJS, 201, 19
Dupuy, T. J., Liu, M. C., Allers, K. N., et al. 2018, AJ, 156, 57
Dupuy, T. J., Liu, M. C., & Ireland, M. J. 2009, ApJ, 692, 729
Feiden, G. A. 2016, A&A, 593, A99
Filippazzo, J. C., Rice, E. L., Faherty, J., et al. 2015, ApJ, 810, 158
Gaia Collaboration, Brown, A. G. A., Vallenari, A., et al. 2018, A&A, 616, A1
Gagné, J., Lafrenière, D., Doyon, R., Malo, L., & Artigau, É 2014, ApJ,
   783, 121
Gagné, J., Mamajek, E. E., Malo, L., et al. 2018, ApJ, 856, 23
Galli, P. A. B., Loinard, L., Ortiz-Léon, G. N., et al. 2018, ApJ, 859, 33
Janson, M., Hormuth, F., Bergfors, C., et al. 2012, ApJ, 754, 44
Kenyon, S. J., & Hartmann, L. 1995, ApJS, 101, 117
Kraus, A. L., Cody, A. M., Covey, K. R., et al. 2015, ApJ, 807, 3
Kraus, A. L., Shkolnik, E. L., Allers, K. N., & Liu, M. C. 2014, AJ, 147, 146
Lagrange, A.-M., Boccaletti, A., Langlois, M., et al. 2019, A&A, 621, L8
Lagrange, A.-M., Bonnefoy, M., Chauvin, G., et al. 2010, Sci, 329, 57
Lee, J., & Song, I. 2019, MNRAS, 486, 3434
Lee, J.-J. 2015, plp: Version 2.0, Zenodo, doi:10.5281/zenodo.18579
Lee, J.-J., Gullikson, K., & Kaplan, K. 2017, igrins/plp 2.2.0, Zenodo, doi:10.
   5281/zenodo.845059
Liu, M. C. 2004, Sci, 305, 1442
Liu, M. C., Dupuy, T. J., & Allers, K. N. 2016, ApJ, 833, 96
López-Valdivia, R., Mace, G. N., Sokal, K. R., et al. 2019, ApJ, 879, 105
Lowrance, P. J., Schneider, G., Kirkpatrick, J. D., et al. 2000, ApJ, 541, 390
Macintosh, B., Graham, J. R., Barman, T., et al. 2015, Sci, 350, 64
Macintosh, B., Graham, J. R., Ingraham, P., et al. 2014, PNAS, 111, 12661
Maire, A. L., Bonnefoy, M., Ginski, C., et al. 2016, A&A, 587, A56
Males, J. R., Close, L. M., Miller, K., et al. 2018, Proc. SPIE, 10703, 1070309
Malo, L., Doyon, R., Feiden, G. A., et al. 2014, ApJ, 792, 37
Mamajek, E. E., & Bell, C. P. M. 2014, MNRAS, 445, 2169
Mann, A. W., Gaidos, E., Mace, G. N., et al. 2016, ApJ, 818, 46
Marois, C., Macintosh, B., Barman, T., et al. 2008, Sci, 322, 1348
Martinache, F., Guyon, O., Jovanovic, N., et al. 2014, PASP, 126, 565
Messina, S., Lanzafame, A. C., Malo, L., et al. 2017, A&A, 607, A3
Montet, B. T., Bowler, B. P., Shkolnik, E. L., et al. 2015, ApJL, 813, L11
Mugrauer, M., Vogt, N., Neuhäuser, R., & Schmidt, T. O. B. 2010, A&A,
Murphy, S. J., Lawson, W. A., & Bessell, M. S. 2013, MNRAS, 435, 1325
Nakajima, T., Oppenheimer, B. R., Kulkarni, S. R., et al. 1995, Natur, 378, 463
Naud, M.-E., Artigau, É, Doyon, R., et al. 2013, EPJWC, 47, 13004
Neuhäuser, R., Ginski, C., Schmidt, T. O. B., & Mugrauer, M. 2011, MNRAS,
Nielsen, E. L., de Rosa, R. J., Wang, J., et al. 2016, AJ, 152, 175
Norton, A. J., Wheatley, P. J., West, R. G., et al. 2007, A&A, 467, 785
Oppenheimer, B. R., Kulkarni, S. R., Matthews, K., & Nakajima, T. 1995, Sci,
   270, 1478
```

```
Park, C., Jaffe, D. T., Yuk, I.-S., et al. 2014, Proc. SPIE, 9147, 91471D
Pöhnl, H., & Paunzen, E. 2010, A&A, 514, A81
Rajan, A., Rameau, J., de Rosa, R. J., et al. 2017, AJ, 154, 10
Rayner, J. T., Toomey, D. W., Onaka, P. M., et al. 2003, PASP, 115, 362
Rebolo, R., Zapatero Osorio, M. R., & Martín, E. L. 1995, Natur, 377, 129
Rizzuto, A. C., Mann, A. W., Vanderburg, A., Kraus, A. L., & Covey, K. R.
   2017, AJ, 154, 224
Saumon, D., & Marley, M. S. 2008, ApJ, 689, 1327
Schlieder, J. E., Lépine, S., & Simon, M. 2010, AJ, 140, 119
Service, M., Lu, J. R., Campbell, R., et al. 2016, PASP, 128, 095004
Shkolnik, E. L., Allers, K. N., Kraus, A. L., Liu, M. C., & Flagg, L. 2017, AJ,
   154, 69
Shkolnik, E. L., Anglada-Escudé, G., Liu, M. C., et al. 2012, ApJ, 758, 56
Simon, M., Guilloteau, S., Beck, T. L., et al. 2019, ApJ, 884, 42
Simons, D. A., & Tokunaga, A. 2002, PASP, 114, 169
Snellen, I. A. G., & Brown, A. G. A. 2018, NatAs, 2, 883
```

```
Song, I., Schneider, G., Zuckerman, B., et al. 2006, ApJ, 652, 724
Tokunaga, A. T., Simons, D. A., & Vacca, W. D. 2002, PASP, 114, 180
Tokunaga, A. T., & Vacca, W. D. 2007, in ASP Conf. Ser. 364, The Future of
  Photometric, Spectrophotometric and Polarimetric Standardization, ed.
  C. Sterken (San Francisco, CA: ASP), 409
Torres, C. A. O., Quast, G. R., da Silva, L., et al. 2006, A&A, 460, 695
Torres, C. A. O., Quast, G. R., Melo, C. H. F., & Sterzik, M. F. 2008, in
  Handbook of Star Forming Regions, Volume II: The Southern Sky, Vol. 5,
  ed. B. Reipurth (San Francisco, CA: ASP), 757
Vacca, W. D., Cushing, M. C., & Rayner, J. T. 2003, PASP, 115, 389
van Dokkum, P. G. 2001, PASP, 113, 1420
Witte, S., Helling, C., Barman, T., Heidrich, N., & Hauschildt, P. H. 2011,
    A&A, 529, A44
Zacharias, N., Finch, C. T., Girard, T. M., et al. 2012, yCat, 1322, 0
Zuckerman, B., & Song, I. 2004, ARA&A, 42, 685
Zuckerman, B., Song, I., Bessell, M. S., & Webb, R. A. 2001, ApJL, 562, L87
```